Technical Report

080

SHIELDING FACTORS FOR UNDERGROUND SHELTERS OF VARIOUS GEOMETRIC SHAPES

5 April 1961

U. S. NAVAL CIVIL ENGINEERING LABORATORY

Port Hueneme, California

SHIELDING FACTORS FOR UNDERGROUND SHELTERS OF VARIOUS GEOMETRIC SHAPES

Y-F011-05-329

Type C

by

J. C. LeDoux, L. K. Donovan

OBJECT OF TASK

To improve existing knowledge of gamma and neutron shielding properties of shelters in order to fill gaps in nuclear shielding knowledge.

ABSTRACT

This study investigates the additional nuclear shielding from an isotropic (plane) radioactive gamma source afforded by various shapes of underground curved-roof shelters compared to the basic slab shield. This additional shielding is defined in the form of a dimensionless Geometry Factor which is a function of the physical dimensions and shape of the shelter.

Curves are presented from which the Geometry Factors for the underground shelter shapes of spheres, horizontal cylinders, ellipsoids, and vertical cylinders or silos can be obtained with minimum calculations using only the physical dimensions of the shelter and the depth of material above the crown of the shelter.

The Geometry Factors thus obtained are independent of material and photon energy except in the case of the silo and can be used as dimensionless factors once the attenuation for a slab shield has been calculated for a particular set of radiological conditions and materials.

CONTENTS

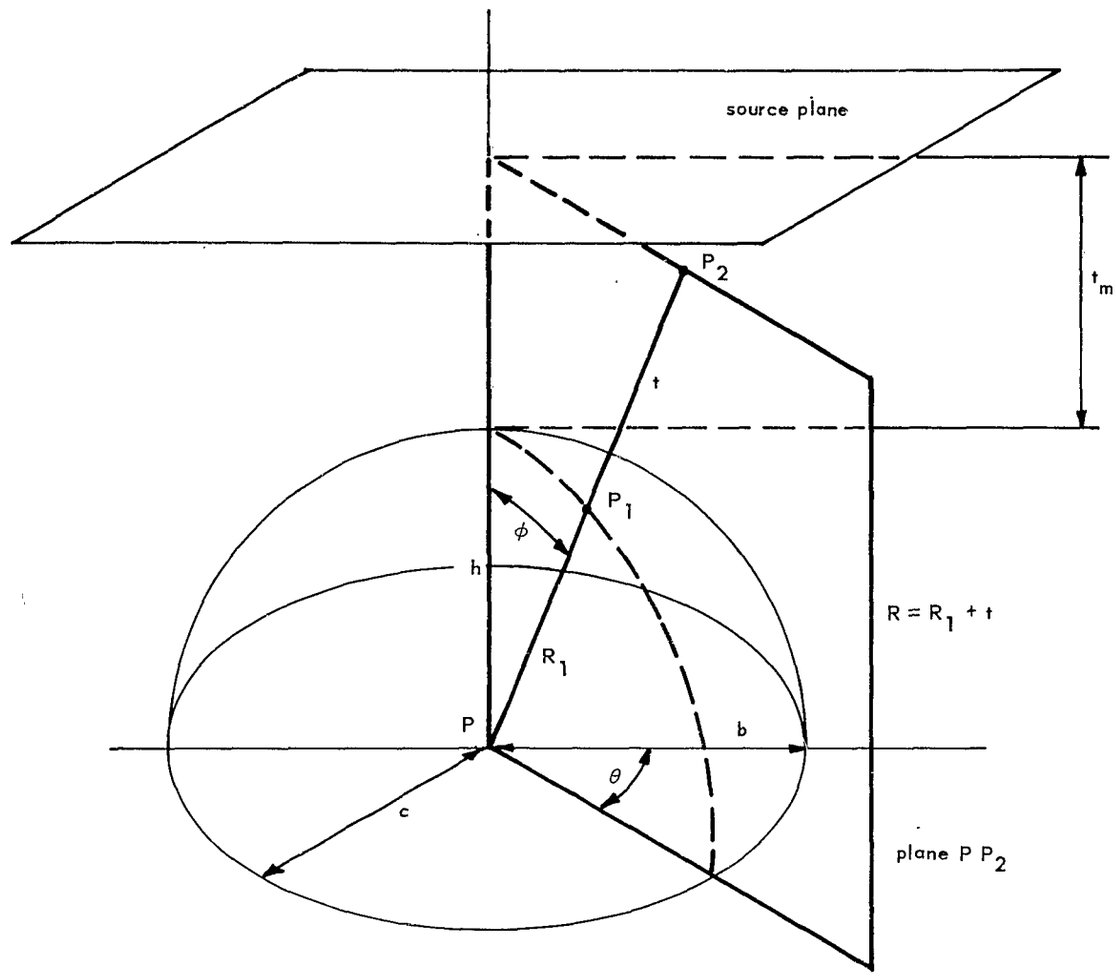

Figure 1. Sketch of most general case considered.

INTRODUCTION

The U. S. Naval Civil Engineering Laboratory is charged by the Bureau of Yards and Docks with the responsibility of developing design principles for the construction of atomic warfare shelters for use by the Naval Shore Establishment.

The simplest shielding configuration for nuclear radiation is a plane slab, and this case has been taken as basic. Much work has been done for slabs with both isotropic and plane collimated sources at various angles of incidence. Since actual underground shelter geometry may be quite different from slab geometry, the shielding effectiveness of other configurations needs to be known. This report is a study of the effectiveness of underground structures of various curved roof shapes as shields.

BASIC ASSUMPTIONS

The following assumptions have been made:

1. The shelter is buried in a semi-infinite mass of earth so that the distance from the crown of the structure to the surface of the ground is t_m.

2. The source of radiation is a plane, equally distributed, isotropic source of gamma photons located on the surface of the ground.

3. The surface of the ground is smooth and infinite in extent.

DESCRIPTION OF THE PROBLEM

It is assumed that there is a shelter buried below an infinite plane source of gamma photons. Figure 1 is a sketch of the most general case considered. This shape is a hemi-ellipsoid whose axis radii are h, b, and c. In all cases only the dose to the central point, P, in the shelter will be considered. One method to determine the total dose to point P from the entire infinite plane is to sum up the contribution from all points in the plane.

Thus, the dose at point P from the differential area dA at point P_2 in the source plane will be:

$$D_2 = \frac{Sf\,dA}{4\pi R^2} B_r e^{-\mu_a R_1 - \mu t} \qquad (1)$$

where: D_2 = dose received at P from P_2, r/hr

S = strength of the gamma source, photons/cm^2-sec

f = conversion factor, r/hr/photons/cm^2-sec

R = distance from source point to detector, cm

B_r = build-up factor for geometry

μ = linear absorption coefficient for soil, cm^{-1}

μ_a = linear absorption coefficient for air, cm^{-1}

t = thickness of soil between source point and detector, cm

R_1 = distance from dose point to surface of shelter, cm

The dose, then, from the entire infinite plane would be:

$$D = \frac{Sf}{2} \int_{h+t_m}^{\infty} B_r e^{-\mu_a R_1 - \mu t} \frac{dR}{R} \qquad (2)$$

Referring to Figure 2, which is the plane section through P and P_2, it can be seen that the shield mass can be considered in two parts: (1) a slab shield of thickness t_m and, (2) an additional mass bounded by the slab shield and the surface of the shelter. The distance t of the exponential term of Equation 2 can be separated into two terms, t_1 and t_2. Regardless of the shape of the shelter, as long as it is concave downward, the value of t_1 can be expressed as a function of t_m and the central angle ϕ since it is symmetrical about the vertical axis, thus:

$$t_1 = t_m \sec \phi \tag{3}$$

By similar reasoning, the distance from the dose point, P, to the underside of the slab shield would be: h secϕ. Converting to spherical coordinates, the distance R_1 (dose point to roof of shelter) would be:

$$R_1 = \left[\frac{\sin^2 \phi \cos^2 \theta}{c^2} + \frac{\sin^2 \phi \sin^2 \theta}{b^2} + \frac{\cos^2 \phi}{h^2} \right]^{-1/2} \tag{4}$$

the distance t in Equation 2 can now be expressed as:

$$t = t_m \sec \phi + h \sec \phi - R_1 \tag{5}$$

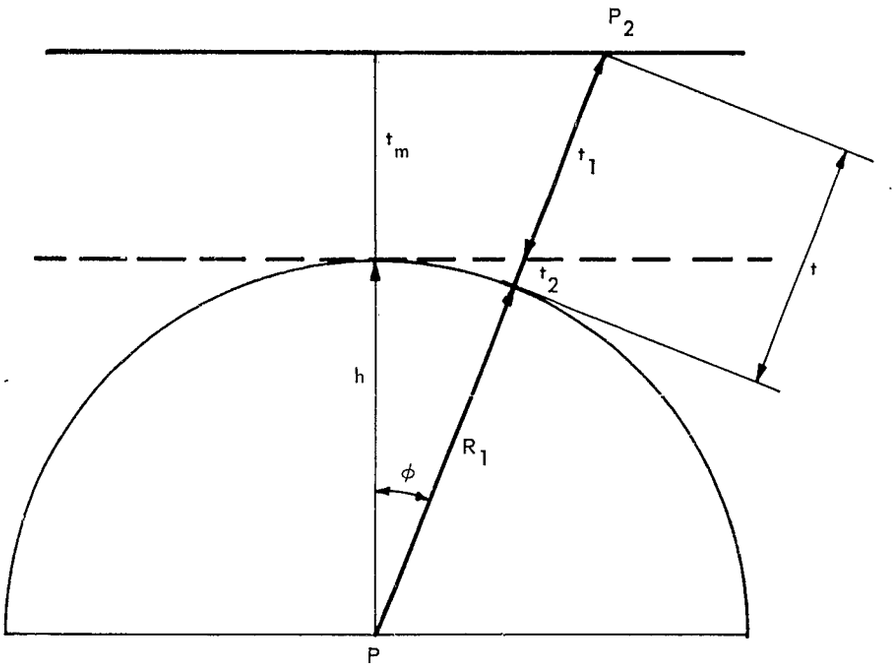

Figure 2. Plane section through points P and P_2 of Figure 1.

Since only concave downward cases will be considered in this report, the special case of the uniform slab shield of infinite extent will provide the least attenuation of the gamma radiation. The slab shield then will be the basic configuration against which all other cases will be compared. The geometry factor, GF, will be defined as:

$$GF = \frac{D_{gs}}{D_s} \tag{6}$$

where: D_{gs} = gamma dose through shield of geometric shape being considered

D_s = gamma dose through slab shield of thickness t_m

Thus, only the factor under the integral sign of Equation 2 need be considered further, since Sf/2 will be common to all cases.

BUILD-UP FACTOR

The build-up factor is the most questionable quantity in the numerical computation of the geometry shielding factors for shelters of various shapes. It has been defined as the ratio of some measurable property of the photon beam (i.e., intensity, number of photons, energy-flux, or biological dose), when the effects of all quanta are included, to the measurable property obtained when only the uncollided flux is considered. Consequently, it is possible for the sake of mathematical development to define the build-up factor in terms of the geometry being considered. A mathematical formula has practical application only when numbers are substituted in it to determine some real quantity. It was necessary therefore to utilize available build-up factors for the numerical integration used in this report.

To arrive at the attenuation integral, an integration or numerical summation over point isotropic sources was used. Consequently, the dose build-up factors for point isotropic sources derived by the moments method were used. [1] These build-up factors were derived from the assumption that the source and detector were located in an infinite, homogeneous medium, and the error involved in applying these build-up factors to finite and even specific geometries must be considered.

In the actual situation being considered, where the detector is located deep in a shelter cavity at some depth within a semi-infinite medium, using point isotropic build-up factors for an infinite medium introduced little if any error. This can be qualitatively explained as follows. The semi-infinite assumption should use a smaller build-up factor than the infinite medium since we are neglecting the photons which are emitted upward from the source and then are scattered back down toward the detector. But since these photons have been scattered at large angles and have been degraded in energy, they will be absorbed sooner than those photons emitted downward toward the detector, and their contribution to the dose at the detector for depths of two mean free paths (at the degraded energy) should be almost negligible. The greatest error would result when a vacuum existed above the semi-infinite medium. In an air-soil medium, photons will also be back-scattered from the air, but the difference then between a soil-soil interface and an air-soil interface should be negligible.

Berger and Doggett [2] have shown that the difference between a finite slab and a semi-infinite slab is also very small. The difference between the two decreases as the photon energy increases and as the thickness of the slab increases. For example, the dose build-up factor for a slab of iron 2 mfp thick and for photon energy of 1 Mev is only 10 percent less than for a semi-infinite medium; for 16 mfp and 10 Mev the difference is only 2 percent.

The situation being considered approaches the semi-infinite medium more than it does the finite slab case, since the soil medium continues below the shelter floor and the minimum shield thickness is 2 mfp. Consequently, for slab geometry the error in using the point isotropic build-up factor is considered to be less than 10 percent. For the other shelter shapes studied, the concave downward geometry approaches the semi-infinite case even more than slab geometry and is equal to the semi-infinite case when the shelter radii equal zero.

Since the end result of this report is the geometry shielding factors obtained by the division of two quantities containing these build-up factors, an inherent error in them would tend to cancel out. Finally, Goldstein [3] indicates that the accuracy of the attenuation coefficient, μ, is even more critical than the build-up factor. He states, "An error of 2% in μ means a 22% change in the unscattered dose at 10 mfp and 50% change at 20 mfp. The uncertainties in the build-up factors are thus overshadowed by those of μ."

BUILD-UP FACTOR APPROXIMATIONS

Goldstein and Wilkins [1] give a specific number for the build-up factors for each photon energy, shield thickness (mfp), and shield material. These numbers can be plotted to give curves of build-up versus energy or versus depth in mfp. In order to handle these functions as part of the uncollided flux equation for gamma photons, the curves must be represented by mathematical equations. If the build-up factor is represented by an exponential equation, the manipulation of the basic equation is simplified since it is also exponential in nature. Taylor [4] recognized this when he postulated the following equation for the build-up function:

$$B_r = A \exp(-\alpha_1 \mu x) + (1 - A) \exp(-\alpha_2 \mu x) \qquad (7)$$

where A, α_1, and α_2 are parameters dependent upon energy and material; and μx is the shield thickness (mfp). Table I lists the values of the parameters A, α_1, and α_2, which Taylor assigned for concrete so that this equation would match the values for the point isotropic build-up factors. Taylor's equation will yield values that are within 5 percent of the values given by Goldstein and Wilkins.

Table I. Values of A, α_1, and α_2 for Concrete and a Point Isotropic Source for the Taylor Build-up Function: $B_r = Ae^{-\alpha_1 \mu x} + (1 - A)e^{-\alpha_2 \mu x}$

Photon Energy, Mev	A	$-\alpha_1$	α_2
0.5	12.5	0.1110	0.0100
1.0	9.9	0.0880	0.0290
2.0	6.3	0.0680	0.0580
4.0	3.9	0.0590	0.0780
6.0	3.1	0.0585	0.0830
8.0	2.7	0.0570	0.0855
10.0	2.6	0.0500	0.0835

Taylor's equation is cumbersome, however, when a numerical calculation must be done. With over 5,000 separate calculations needed to obtain the results of this report, the use of the Taylor equation would have increased this effort by a factor of two.

Consequently, a simpler build-up factor function has been used:

$$B_r = B_o e^{mt} \tag{8}$$

This appears to be an oversimplification, but, for depths of 2 to 20 mfp, it has proved to furnish results within 3 percent of results computed by the Taylor formula. The values of B_o and m were derived as shown in Figure 3. This figure indicates a build-up curve for energy E versus depth in mfp. A straight line is drawn intersecting this curve at 2 and 20 mfp. B_o then is the intersection of this straight line with the axis and is always greater than 1. The slope of the line is m. Since B_o is a constant for a particular energy photon, it can be factored out of the integral. The combination of μ and m results in an "effective" linear attenuation coefficient μ_i. Values of μ_i versus energy are given in Table II. Using this simplified build-up factor formula, all computations could be done on the basis of mean free paths and all data plotted as a function of μt (mfp). Consequently, the photon energy is not required until an actual problem is worked. The geometry shielding factors are valid then for both fallout radiation or initial radiation. Table III is a comparison of the geometry factor for a sphere using the Taylor build-up factor formula and the simplified formula used in this report. The largest error is less than 3 percent.

In view of the fact that the thickness of soil shield being considered will be from a μt of 2 to 20 mean free paths, the attenuation of the gamma photons in the few feet of air within the shelter will not be significant and will be neglected.

Before formulating the general problem, the following substitution will be made:

$$\mu_i = \mu - m$$

$$p = \frac{h}{c}$$

$$q = \frac{h}{b}$$

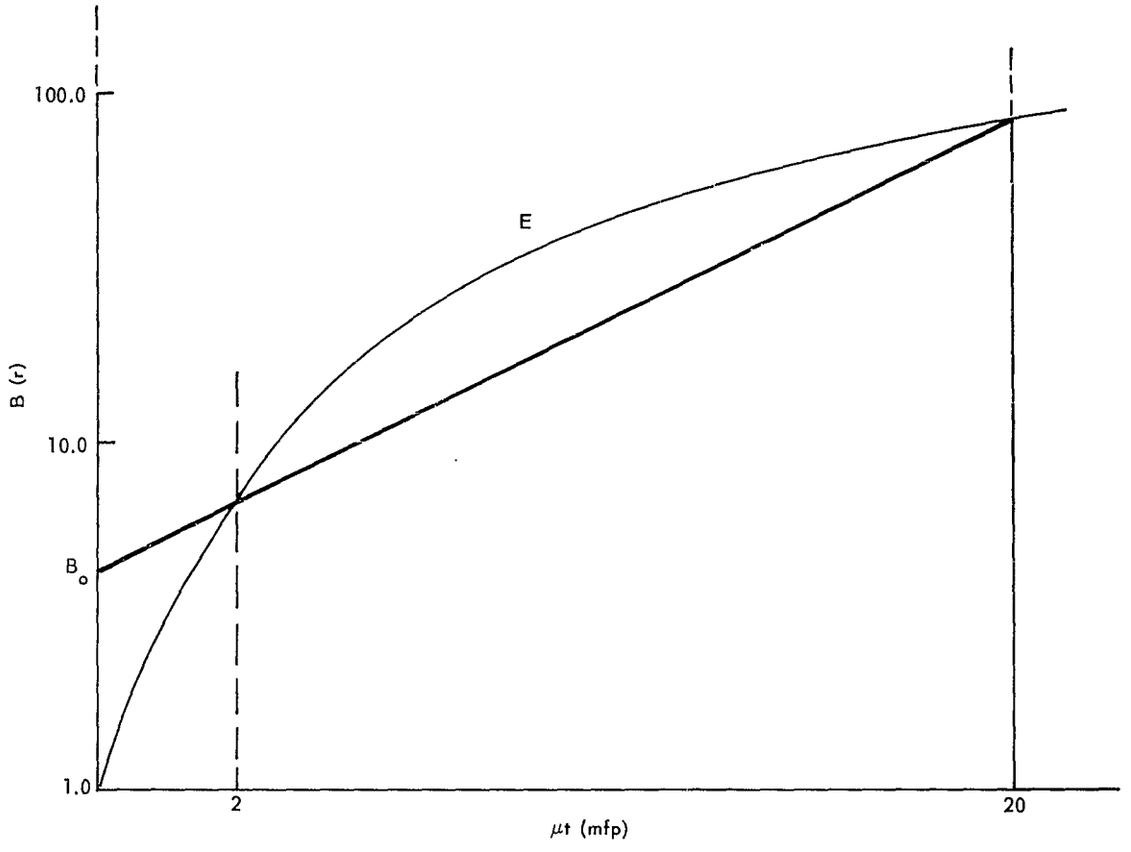

Figure 3. Build-up factor versus material thickness for a particular photon energy.

Table II. Values of μ/ρ, μ, μ_i/ρ, and μ_i for Gamma Photon Energies from 1 to 10 Mev for Soil Density of 1.7 g/cc

Photon	μ/ρ g/cm^2	μ ft^{-1}	μ_i/ρ g/cm^2	μ_i ft^{-1}
1.0	0.0635	3.28	0.0580	3.00
2.0	0.0445	2.30	0.0410	2.12
4.0	0.0317	1.64	0.0290	1.50
6.0	0.0268	1.28	0.0245	1.27
8.0	0.0243	1.25	0.0217	1.12
10.0	0.0229	1.18	0.0200	1.03

Table III. Comparison of $B = B_o e^{mt}$ and $B = Ae^{-\alpha_1 \mu x} + Be^{-\alpha_2 \mu x}$

E	μt	μh	GF	GF Errors	% Errors
1.00	2	10	0.225	0.220	-2.2
1.00	6	10	0.414	0.425	+2.1
1.00	10	10	0.524	0.540	+2.9
6.00	2	10	0.220	0.220	0
6.00	6	10	0.435	0.425	-2.3
6.00	10	10	0.526	0.540	+2.6
1.00	2	15	0.167	0.165	-1.2
1.00	2	20	0.132	0.130	-1.5

We will now define I as the integral portion of Equation 2. The $SfB_o/2$ is dropped since it is a common factor for all cases. Thus, the general case can be represented by:

$$\mathrm{I} = \int_{h + t_m}^{\infty} \exp^{-1} \left[\mu_i t_m \sec \phi + \mu_i h \left\{ \sec \phi - (p^2 \sin^2 \phi \cos^2 \theta + q^2 \sin^2 \phi \sin^2 \theta + \cos^2 \phi)^{-1/2} \right\} \right] \frac{dR}{R} \tag{9}$$

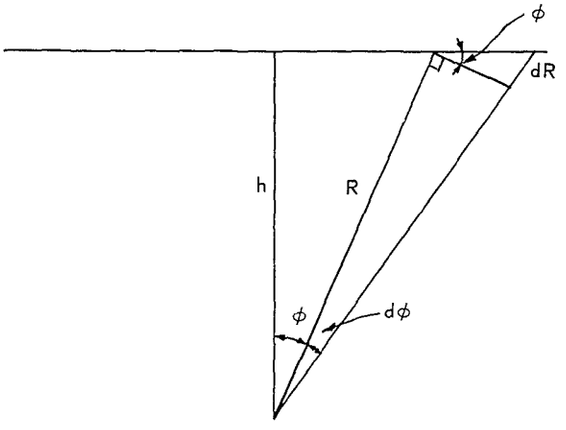

Figure 4. Schematic section of shelter dimensions.

Using Figure 4, it can be shown that for small increments of d ϕ the following identity holds:

$$\tan \phi \; d\phi = \frac{dR}{R} \tag{10}$$

Letting $F(\phi, \theta) = p^2 \sin^2\phi \cos^2\theta + q^2 \sin^2\phi \sin^2\theta + \cos^2\phi$, Equation 9 becomes:

$$I = \int_{h + t_m}^{\infty} \exp^{-1} \left[\mu_i t_m \sec\phi + \mu_i h \sec\phi - \mu_i h F(\phi, \theta) \right] \tan\phi \, d\phi \quad (11)$$

Specific Cases: Referring back to Figure 2, the values of t_1 and t_2 are:

$$t_1 = t_m \sec\phi$$

$$t_2 = h \left[\sec\phi - F(\phi, \theta) \right]$$

The various specific cases can now be generated by assigning specific values to p and q. The cases considered in this report are:

(1) Slab: $p = q = 0$

$$t_1 = t_m \sec\phi$$

$$t_2 = 0$$

(2) Sphere: $p = q = 1$

$$t_1 = t_m \sec\phi$$

$$t_2 = h (\sec\phi - 1)$$

(3) Horizontal Cylinder:

$$p = 0,\ q = 1$$

$$t_1 = t_m \sec\phi$$

$$t_2 = h\left[\sec\phi - (\sin^2\phi \sin^2\theta + \cos^2\phi)^{-1/2}\right]$$

(4) Paraboloid:

$$p = q \neq 1 \neq 0$$

$$t_1 = t_m \sec\phi$$

$$t_2 = h\left[\sec\phi - (q^2 \sin^2\phi + \cos^2\phi)^{-1/2}\right]$$

(5) Ellipsoid:

$$p \neq q \neq 1 \neq 0$$

$$t_1 = t_m \sec\phi$$

$$t_2 = h\left[\sec\phi - (p^2 \sin^2\phi \cos^2\theta + q^2 \sin^2\phi \sin^2\theta + \cos^2\phi)^{-1/2}\right]$$

(6) Vertical Cylinder: See Appendix A.

SOLUTION OF THE PROBLEM

Numerical Integration

The solution of Equation 11 is desired for the various specific cases being considered. An exact solution by integration is only possible for the simple slab and spherical cases. For the others, numerical integration must be used. In order to perform this integration the source plane will be divided into a number of concentric rings, centered over the dose point, P. Each of these rings will be determined

by the central angle ϕ to account for the dependence of the equation on ϕ. The plane will be further divided into sectors to provide for the dependence on the angle θ. This is illustrated by Figure 5. Each small area will then be considered as a separate dose source area, as indicated in Figure 5, Area A_n. This area is defined by the angles, $\phi_n - \phi_{n+1}$; $\theta_n - \theta_{n+1}$.

For purposes of the numerical integration, equal angle increments of 5 degrees for ϕ were used up to 65 degrees (contributions no longer significant), and 15-degree sectors were used for θ. The numerical integration was checked against the exact integration (Table IV) for the slab and sphere cases to test the accuracy of using the 5-degree increments. The error was less than one percent. This is sufficiently accurate for the purpose of this study. Again the fact that the slab case is used as a basis of comparison for all other cases would tend to cancel out any error involved.

Table IV. Comparison of Exact and Numerical Integrations for Slab and Sphere Cases

μt_m	SLAB		SPHERE	
	Exact	Numerical	Exact	Numerical
2	4.89×10^{-2}	4.88×10^{-2}	1.04×10^{-2}	1.04×10^{-2}
4	3.78×10^{-3}	3.77×10^{-3}	1.21×10^{-3}	1.21×10^{-3}
6	3.60×10^{-4}	3.58×10^{-4}	1.47×10^{-4}	1.45×10^{-4}
8	3.76×10^{-5}	3.74×10^{-5}	1.76×10^{-5}	1.75×10^{-5}
10	4.16×10^{-6}	4.13×10^{-6}	2.16×10^{-6}	2.14×10^{-6}

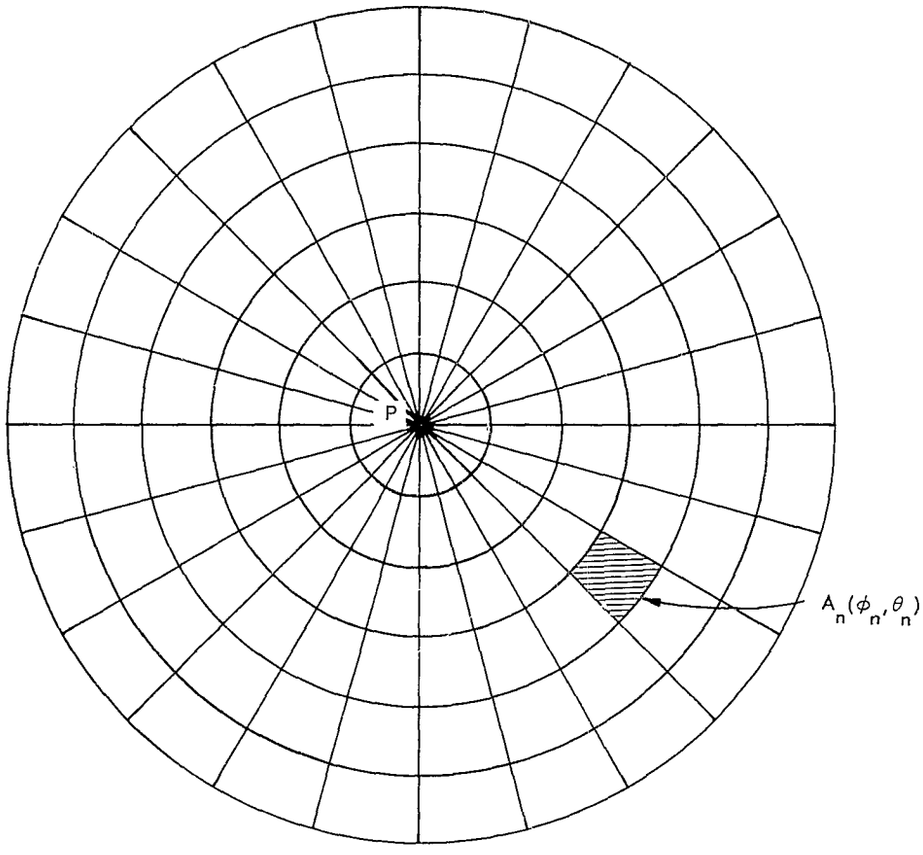

Figure 5. Area division of slab source for integration purposes.

Exact Integration

The integrations of the slab and sphere, based on the same general assumptions which have been made for this study, have been done previously in NCEL Report TR-025 by J. C. LeDoux, [5] and are merely presented below:

$$D\ (\text{Slab}) = \frac{Sf\ B_o}{2}\ E_1\ (\mu_i\ t_m) \tag{12}$$

$$D\ (\text{Sphere}) = \frac{Sf\ B_o}{2}\ e^{\mu_i h}\ E_1\ (\mu_i\ R_m) \tag{13}$$

where $E_1\ (\mu_i\ t_m)$ and $E_1\ (\mu_i\ R_m)$ are exponential integrals of the general form,

$$E_1\ (\mu x) = \int_{\mu x}^{\infty} \frac{e^{-t}\ dt}{t}$$

and:

$$R_m = h + t_m$$

These solutions were used to check the numerical integrations for the same cases in order to check the accuracy of the results and the choice of the 5-degree increment. Table IV is a comparison of the exact integration and the numerical integration. The constant factor $SfB_o/2$ has not been included in either case. The difference in all cases is less than one percent. Based on this comparison, it is assumed that comparable accuracy is maintained for all other cases.

GEOMETRY FACTOR CURVES

The geometry factors (GF) for various shapes, semi-ellipsoid, horizontal cylinders, and vertical cylinders are presented in the form of curves.

Ellipsoids

Figure 6 is a curve which fits the data for the ellipsoid-type shelter. It has a maximum error of 10 percent and an average error of 1.0 percent from the computed data (Appendix A). The curve is a plot of GF vs $t/(t + Fh)$, where t is the depth of earth cover over the crown of the shelter arch, h is the height of the shelter, and F is an empirical factor which depends on the ratio of the height of the shelter to the major and minor axis radii of the floor ellipse. This function, $t/(t + Fh)$, was used since it produced the best grouping of the ellipsoid data on a single curve. The derivation of this function is described in Appendix A.

F is obtained by entering the value of $(p^2 + q^2)/2$ in Figure 7.

where: $p = \frac{h}{c}$

$q = \frac{h}{b}$

and: c = the major axis radius

b = the minor axis radius

The curve (Figure 6) is also valid for a sphere or a slab, since $F = 1$ for a sphere, and $F = 0$ for a slab.

Horizontal Cylinders

Figure 8 is a curve of GF vs $t/(t + Fh)$ for shelters of the horizontal cylinder type. This horizontal cylinder does not have to have a uniform radius. F in this case is:

$$F = \frac{p^2}{2}$$

since: $q = 0$

where: $p = \frac{h}{c}$

and: h = height of shelter

c = horizontal distance from center of shelter floor to outside arch

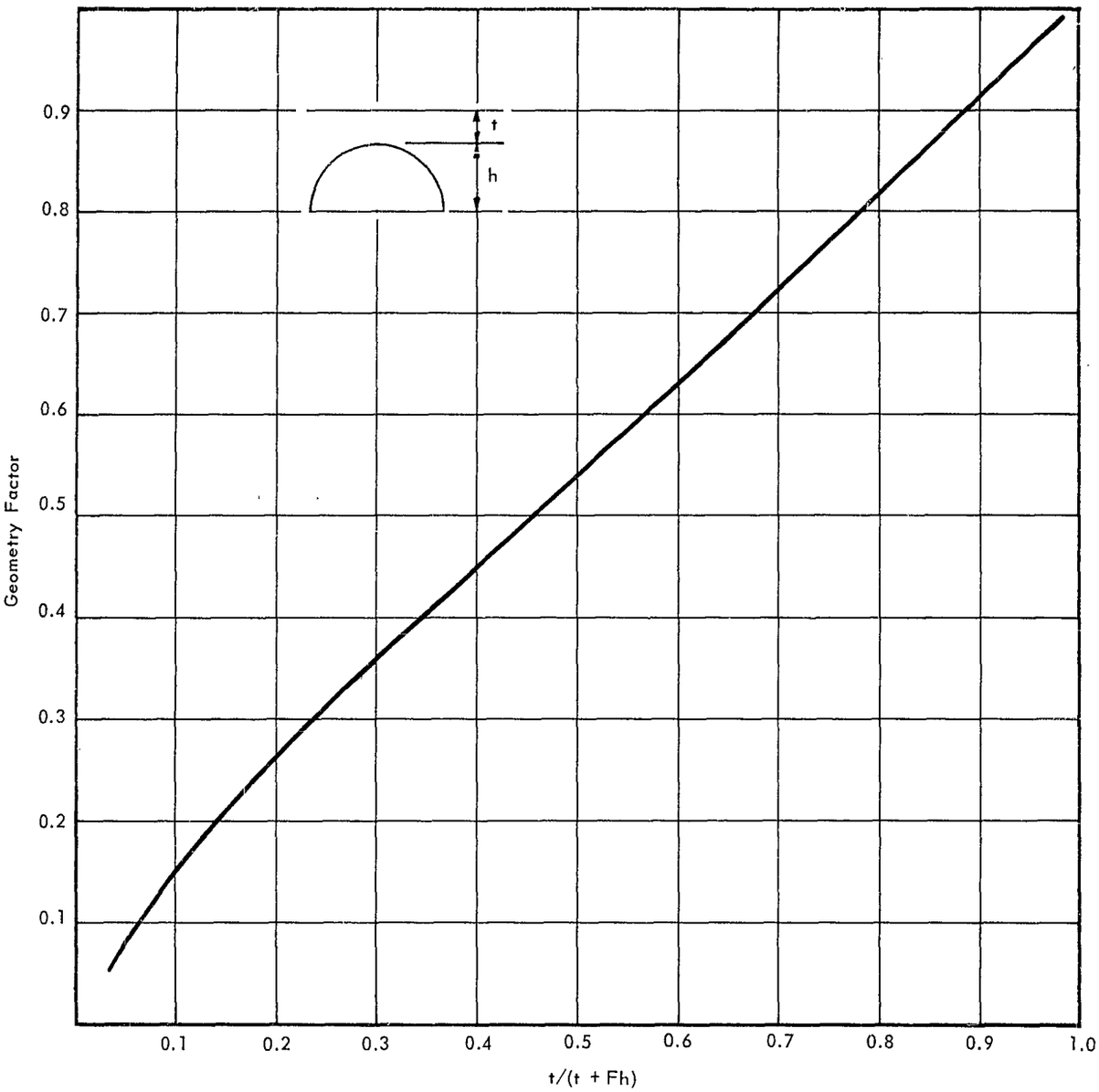

Figure 6. Geometry factors for ellipsoid type shelters vs $t/(t + Fh)$, where $F = \phi \left[(p^2 + q^2)/2\right]$ from Figure 7.

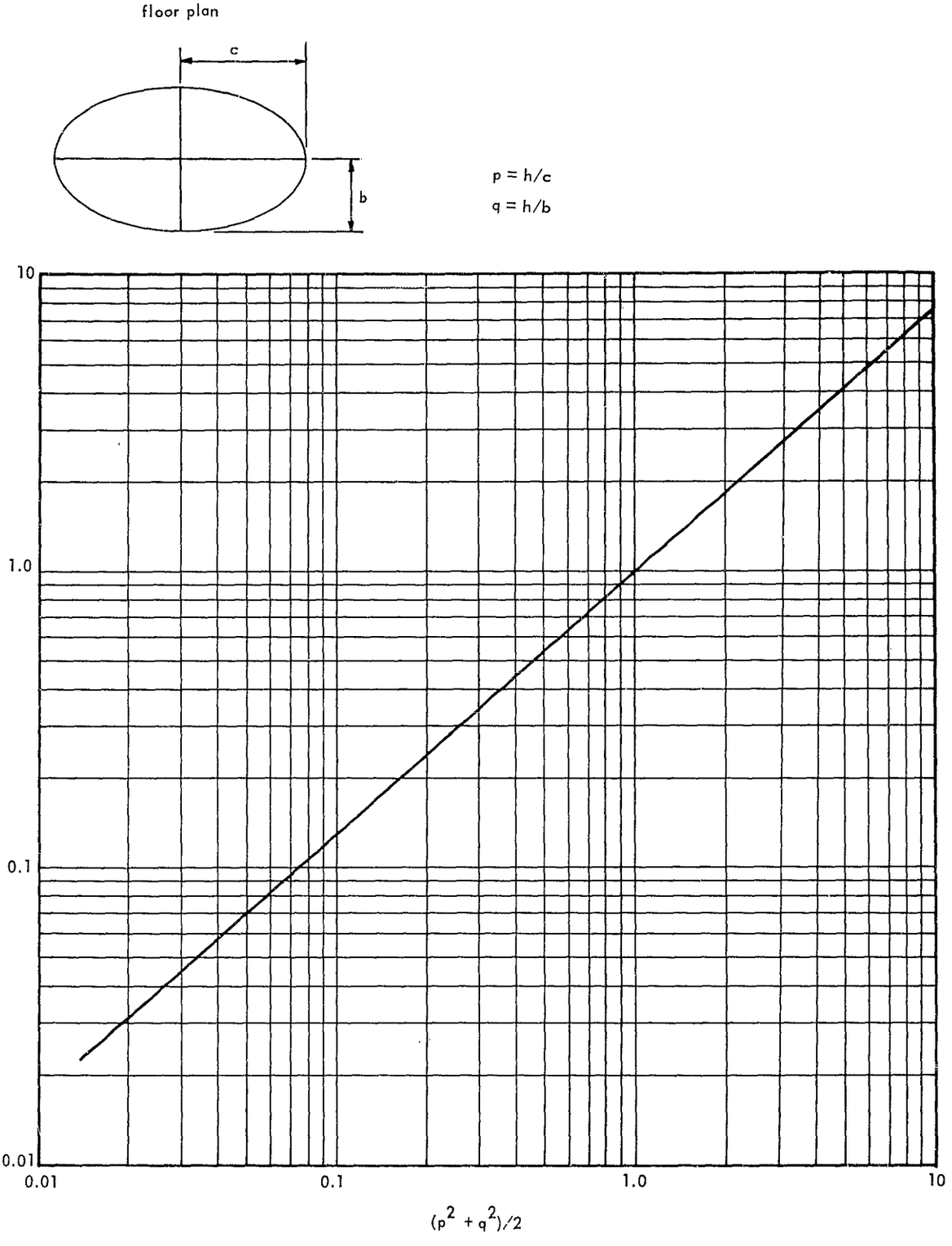

Figure 7. Factor F vs $(p^2 + q^2)/2$.

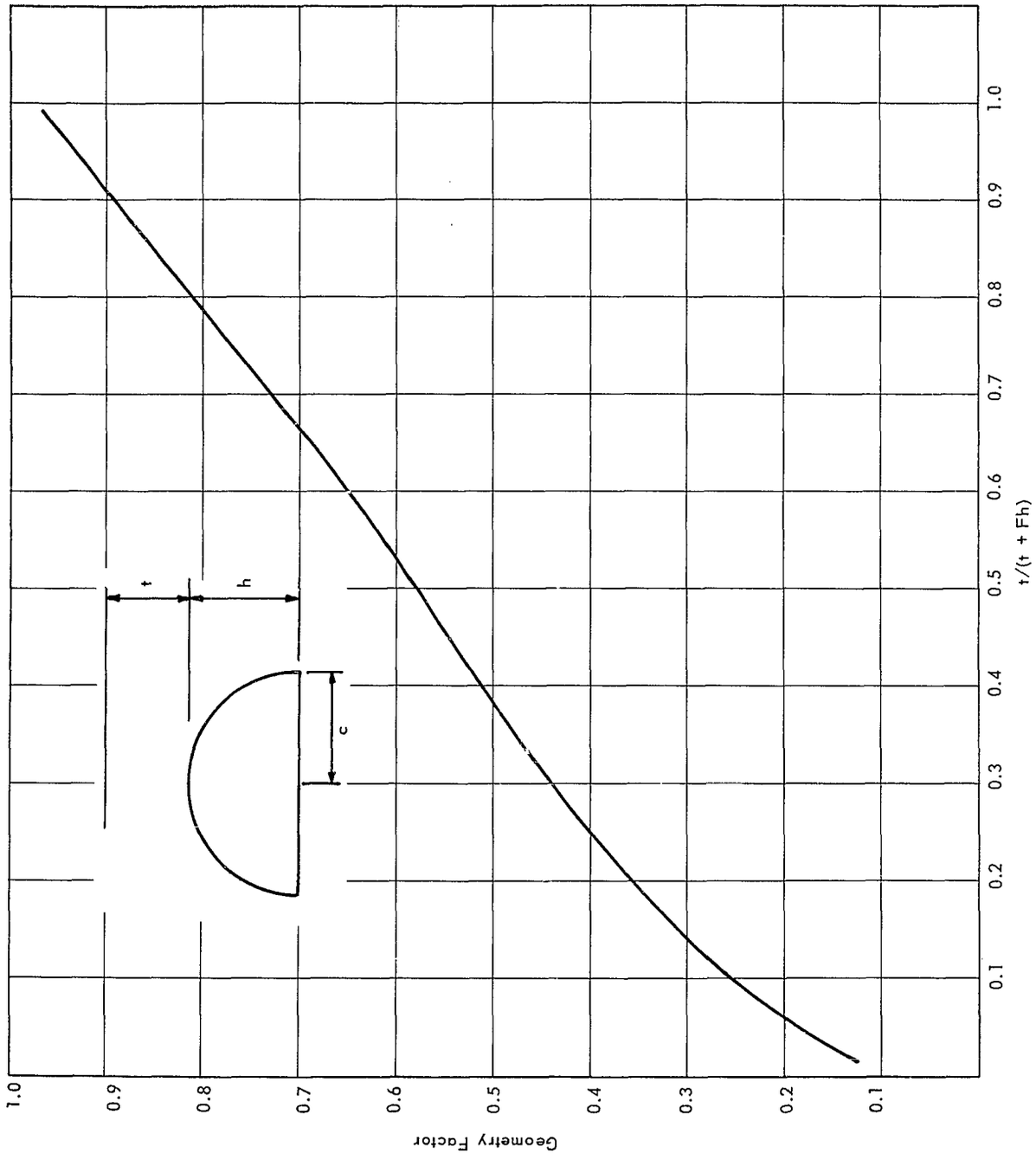

Figure 8. Geometry factors for horizontal cylinders vs $t/(t + Fh)$; where $F = p^2/2$, and $p = h/c$.

Vertical Cylinders

Figure 9 is a plot of the GF for vertical cylinders (silos) vs r_o/h for various values of μ_i t, where r_o is the radius of the cylinder, h is the height of the cylinder, and μ_i t is the mean free paths of soil above the roof of the silo. The vertical silo case takes into account radiation coming from the roof and also from the sides. Appendix A points out that if the roof contribution alone is considered as the contributing source, the maximum error would be only 5 percent. Thus, the OCDM manual for aboveground structures could be used for silos using only the roof contribution.

Examples

Some examples of geometry factors for various exact shapes using Figures 6, 8, and 9 are given in Appendix B.

CONCLUSIONS

The geometry factor, which has been derived in this report, can now be used to determine the additional nuclear shielding provided by the physical shape of concave downward underground structures as compared to a simple slab shield. The merits of one shape can be evaluated against that of another and the best one chosen on the basis of its shielding, consistent with the blast design.

RECOMMENDATION

It is recommended that limited experiments be performed to verify the results of this theoretical study.

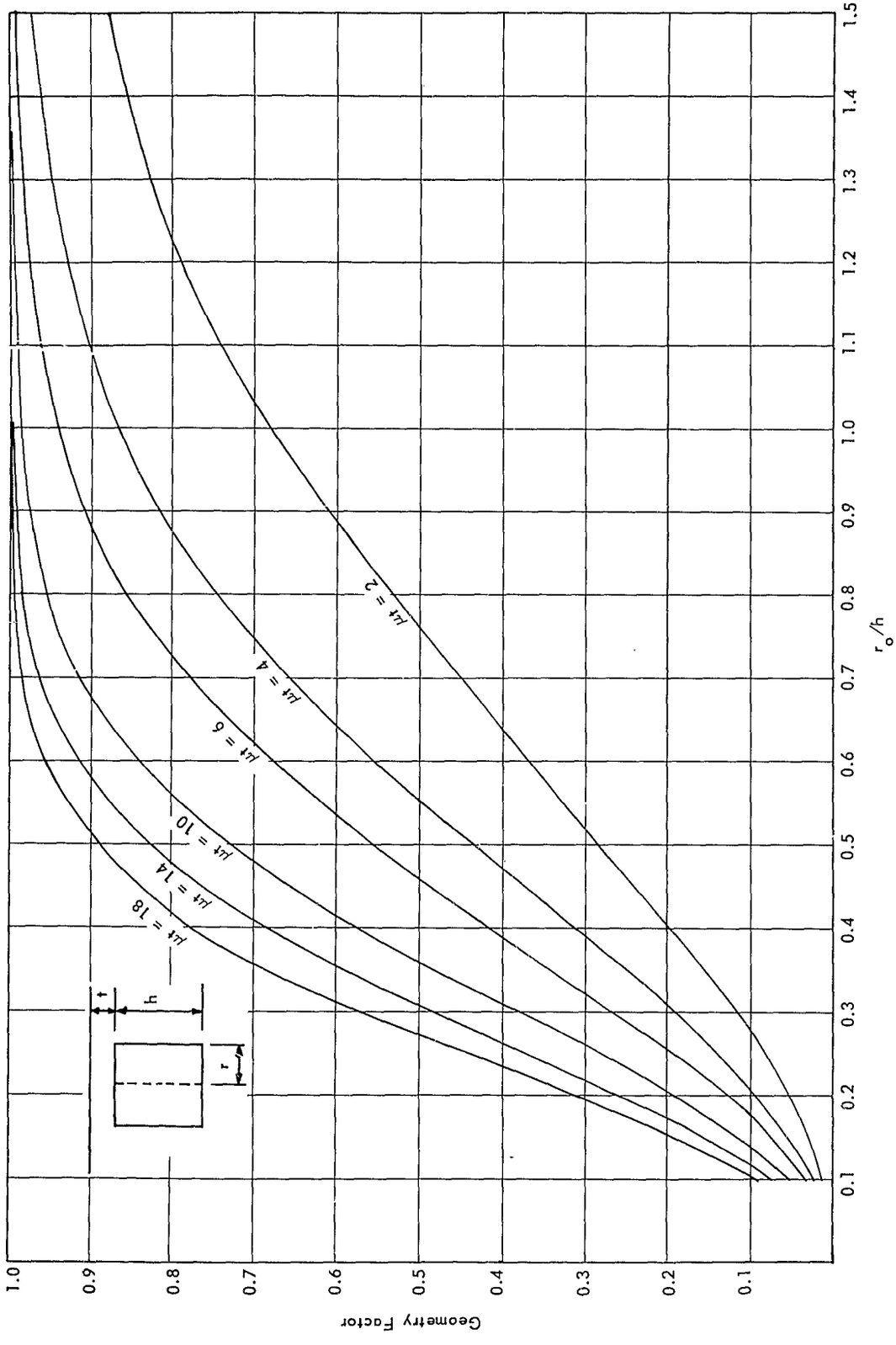

Figure 9. Geometry factors for underground vertical silos vs r_o/h.

REFERENCES

1. U. S. Atomic Energy Commission. NYO-2075, Calculations of the Penetration of Gamma Rays, by Herbert Goldstein and J. Ernest Wilkins. White Plains, New York, 30 June 1954.

2. Berger, M. J., and J. Doggett. "Reflection and Transmission of Gamma Radiation by Barriers: Semianalytic Monte Carlo Calculations." Journal of Research, National Bureau of Standards, 56:89C (1956).

3. Goldstein, J. Fundamental Aspects of Reactor Shielding. Addison Wesley Publishing Company, Reading, Massachusetts, 1959. Chapter 5.

4. Bettis Atomic Power Laboratory. WAPD-Memo-RM-217, Applications of Gamma Ray Build-Up Data to Shield Design, by J. J. Taylor. Pittsburgh, Pennsylvania, 25 June 1954.

5. U. S. Naval Civil Engineering Laboratory. TR-025, Nuclear Radiation Shielding Provided by Buried Shelters, by J. C. LeDoux. Port Hueneme, California, 27 October 1959.

Appendix A

REDUCTION OF DATA

SPHERE, HORIZONTAL CYLINDER, AND ELLIPSOID DEVELOPMENTS

All of the machine calculations are presented in Tables V and VI. This is merely the tabulation of the solution of Equation 11 for the various cases. This data is then used to calculate geometry factors (Tables VII — IX) for the various cases considered.

In order to make the results more useful, it would be advantageous if the geometry factor could be plotted as some function of the various parameters upon which it depends; i.e., h, t_m, p, q, and μ_i. The only cases which can be integrated exactly are the slab and hemisphere. Consequently, an exact expression for the geometry factor for a sphere can be obtained. Using Equations 12 and 13, we find that the geometry factor for a sphere is:

$$GF = \frac{e^{\mu_i h} E_1(\mu_i R_m)}{E_1(\mu_i t_m)}$$

If we let: $E_1(x) = \frac{e^{-x}}{x} F(x)$

then:
$$GF = \frac{\mu_i t_m}{\mu_i t_m + \mu_i h} \left[\frac{F(\mu_i R_m)}{F(\mu_i t_m)}\right] \qquad (14)$$

since: $\frac{F(\mu_i R_m)}{F(\mu_i t_m)} \cong 1$, the geometry factor for a sphere would be:

$$GF \cong \frac{t_m}{(t_m + h)} \qquad (15)$$

This is the same geometry factor previously derived in Reference 5 for a sphere.

It is assumed that the GF for other shapes would have a form similar to Equation 15. The actual attenuation integral (Equation 11) is very complex so that it is impossible to reduce the data to a simple mathematical equation such as Equation 15.

We do know that Equation 15 very closely satisfies the GF for a sphere. The GF for a slab is equal to one by definition. Equation 15 can be modified to satisfy a slab by the introduction of a factor F, thus:

$$GF = \frac{t_m}{(t_m + Fh)} \tag{16}$$

where: F = 0 for a slab, or 1 for a sphere

If we examine Equation 11 further we notice that it depends also on the factors p^2 and q^2. F is actually some perturbation on the height of the shelter h and therefore should depend on the p^2 and q^2 values in some fashion. Let us try:

$$F = \frac{(p^2 + q^2)}{2} \tag{17}$$

This satisfies the slab and sphere conditions since:

$$p = q = 0 \quad \text{for a slab}$$

$$p = q = 1 \quad \text{for a sphere}$$

Using Equation 17, a plot of GF versus $t/(t + Fh)$, where t will now be used for t_m, shows that the computed data for horizontal cylinders is satisfied by this function of F, since all points plot very close to a single line (Figure 10). The best fit of these points has been used to produce Figure 8.

The data for the ellipsoid and silo cases scatters considerably from a single line. In order to determine if F could be represented by some other function besides Equation 17, a plot was made of Equation 16 choosing values of F ranging from 0.01 to 10 for a μh of 10, and for various values of $\mu_i t$. Figure 11 is this plot. Now if the computed values of GF from Table VII are plotted on these curves, we find that they plot as nearly horizontal lines. This means that there is some constant value of F which satisfies the various ellipsoidal cases.

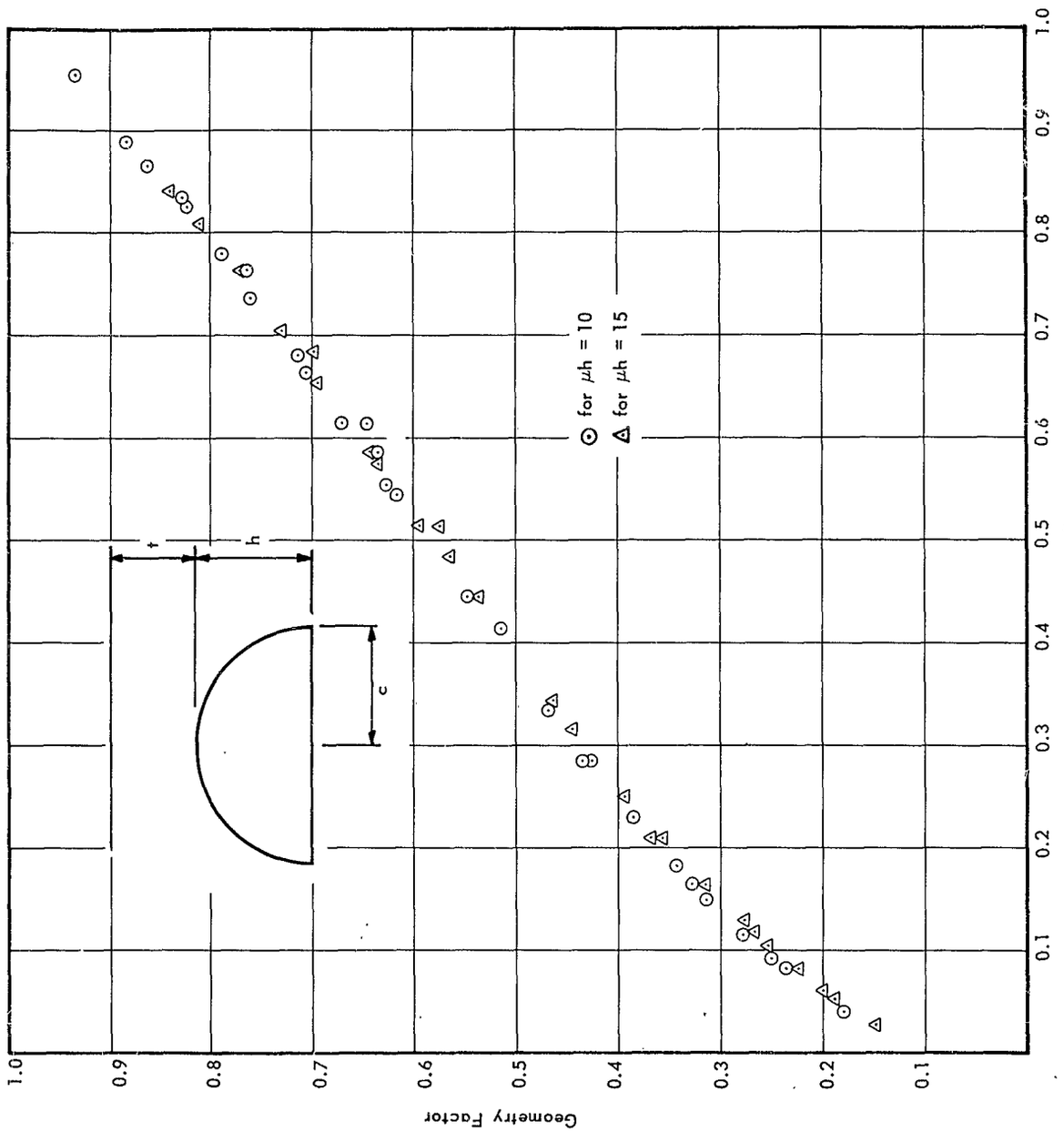

Figure 10. GF vs t/(t + F'h) for horizontal cylinders; where $F' = p^2/2$ and $p = h/c$.

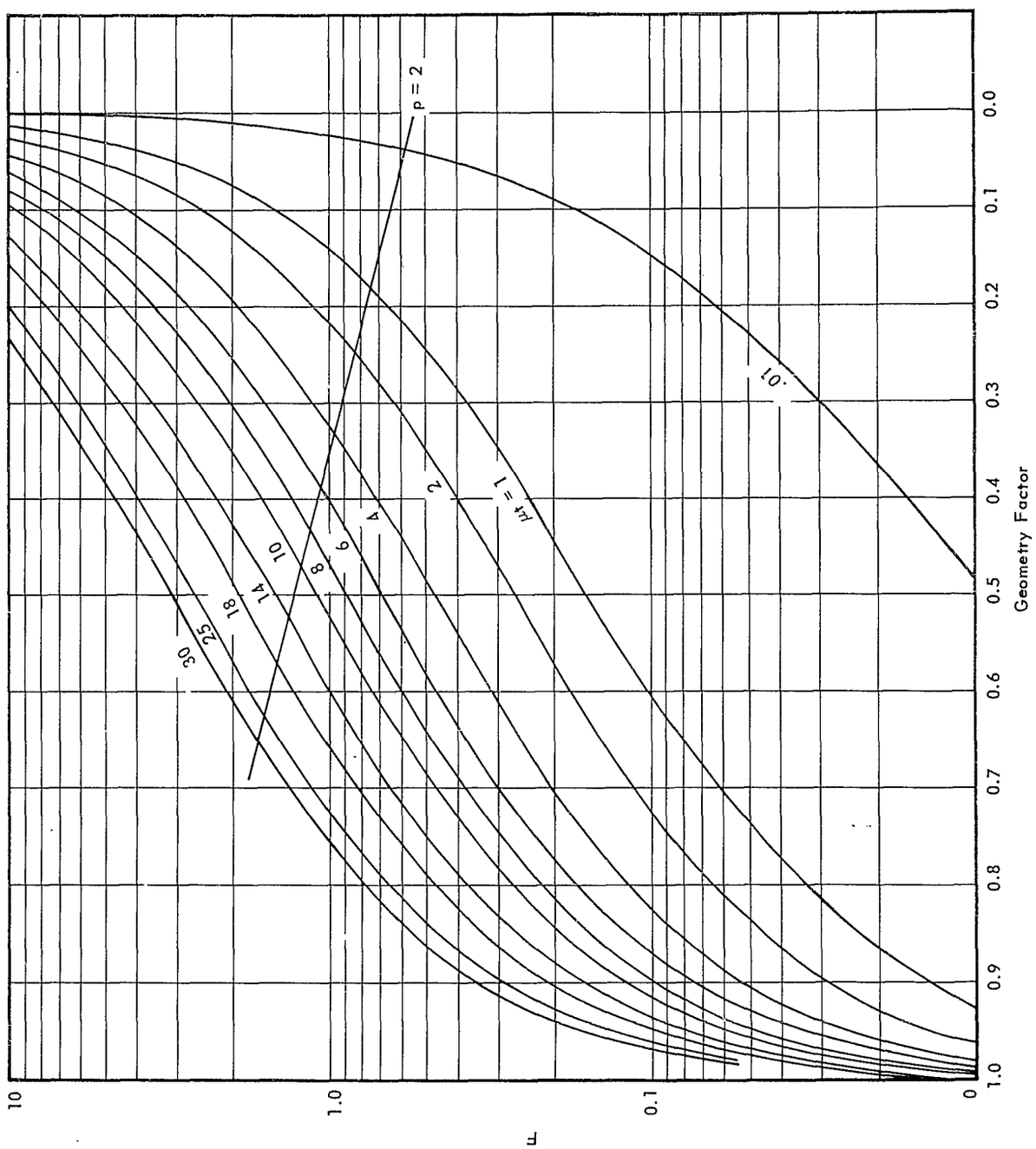

Figure 11. GF vs F for various values of $\mu_1 t$; where $F = (p^2 + q^2)/2$.

This value of F was then plotted against the first guess, $(p^2 + q^2)/2$, and yielded a straight line on log log graph paper, Figure 7. Using the values of F from Figure 7 in Equation 16 brought the values for ellipsoidal shelters close to a straight line, Figure 12. The best fit through these points is the curve of Figure 6. The best fit has a maximum error of 10 percent and an average error of one percent from the computed data.

Computed values of GF for a μh of 15 are listed in Table VIII.

VERTICAL SILO DEVELOPMENT

In the case of the vertical silo, it can be seen from Figure 13 that $t_2 = 0$ when $\phi \leq \phi_c$ and that $t_2 = h \sec\phi - r_o \csc\phi$ when ϕ is greater than ϕ_c where $\phi_c = \arctan r_o/h$.

Therefore, the integration for various values of r_o and h was done in two parts. Consider first when $\phi \leq \phi_c$ and $t_2 = 0$. Equation 11 is greatly simplified:

$$I = \int_{h + t_m}^{\infty} \exp^{-1} (\mu_i t_m \sec\phi) \frac{d R}{R} \tag{18}$$

where: $R = R_1 + t_1$

from Figure 13: $\sec\phi = \dfrac{R}{h + t_m}$

Now let: $\mu_j = \dfrac{\mu_i t_m}{h + t_m}$

Then Equation 18 becomes:

$$I = \int_{h + t_m}^{(h + t_m) \sec\phi} \exp^{-1} (\mu_j R) \frac{d (\mu_j R)}{\mu_j R} \tag{19}$$

which is the form of the exponential integral. It can be easily shown then that:

$$I = E_1 \left[\mu_i (h + t_m) \right] - E_1 \left[\mu_i (h + t_m) \right] \sec \phi \qquad (20)$$

Substituting for the value of μ_i in Equation 20 we have:

$$I = E_1 (\mu_i t_m) - E_1 (\mu_i t_m \sec \phi) \qquad (21)$$

Now let us consider when $\phi > \phi_c$. Equation 11 becomes:

$$I = \int_{(h + t_m) \sec \phi}^{\infty} \exp \left[-\mu_i (t_m + h) \sec \phi + \mu_i r_o \csc \phi \right] \frac{dR}{R} \qquad (22)$$

Now if we let $dR/R = \tan \phi \, d\phi$ as before, then Equation 22 becomes:

$$I = \int_{\phi_c}^{\infty} \exp \left[-\mu_i (t_m + h) \sec \phi + \mu_i r_o \csc \phi \right] \tan \phi \, d\phi \qquad (23)$$

Equation 23 was numerically integrated by machine, using increments for ϕ of 5 degrees until the contribution was negligible. The sum of the results from Equation 23 and Equation 21 for each case was divided by the slab case $E_1 (\mu_i t_m)$ in order to give the geometry factors as defined above.

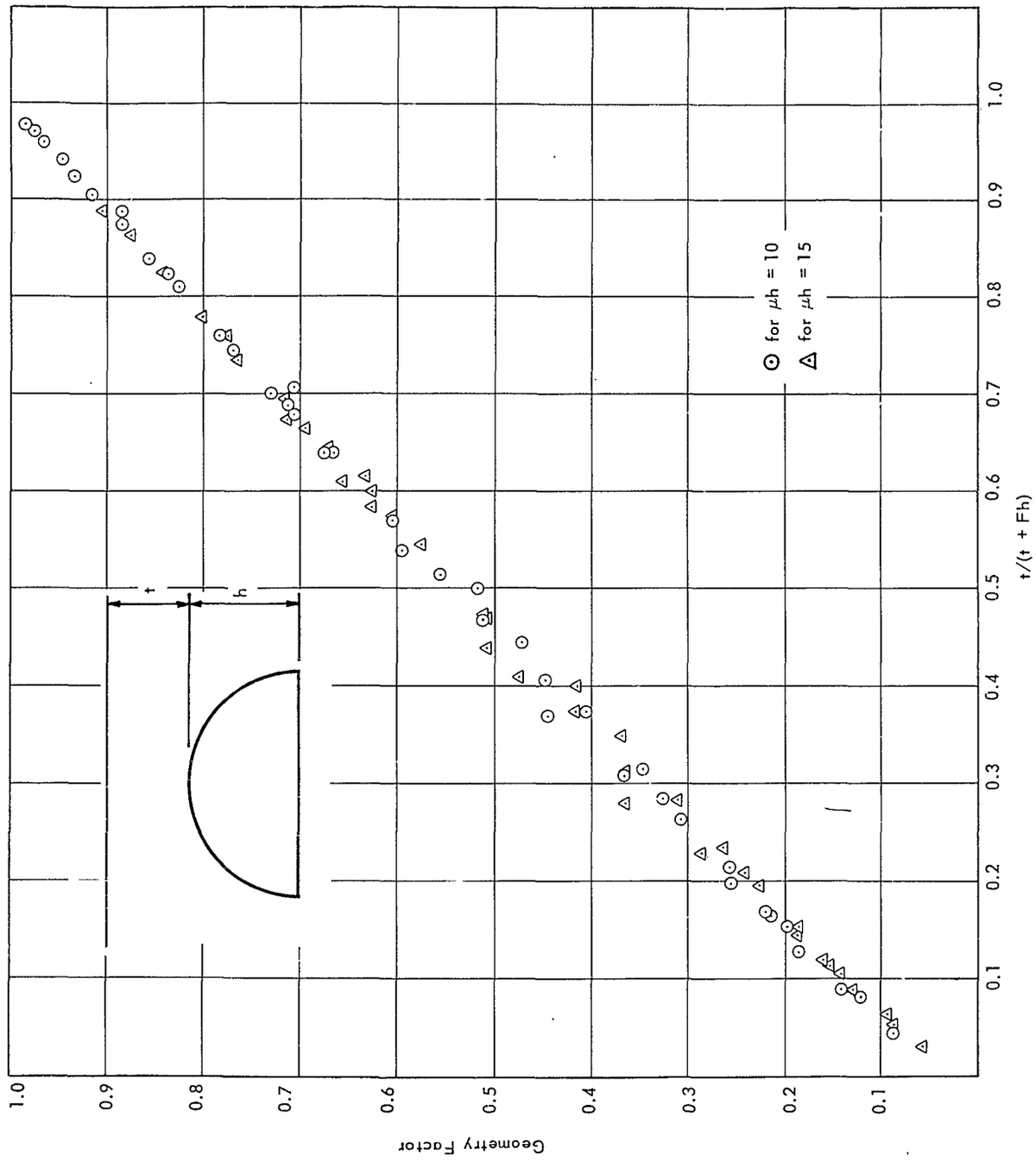

Figure 12. GF vs t/(t + Fh) for ellipsoidal shapes; where $F = \phi \left[(p^2 + q^2)/2 \right]$ from Figure 7.

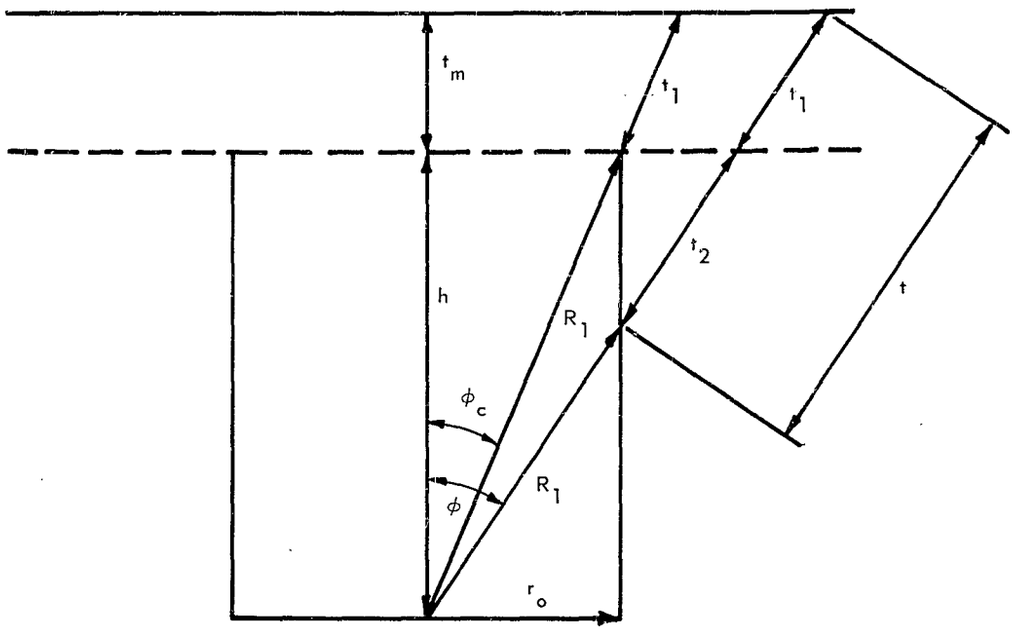

Figure 13. Schematic of vertical silo configuration.

Table IX lists the geometry factors obtained for various values of r_o, h, and μ_i t_m. Figure 9 graphically displays the results, plotting geometry factor versus the ratio r_o/h for various thicknesses of material in mfp. The last column of Table IX is the geometry factor when only Equation 21 is used. It can be seen that the largest variation is only 5 percent, occurring at one of the less important cases.

The value of μ_i t_m is calculated for the particular energy involved. Table II lists the values of μ_i/ρ, and μ_i for soil of density 1.7 gm/cc versus photon energy. Knowing the density of the soil to be used and multiplying μ_i/ρ by this density, μ_i t_m can be calculated in any appropriate units for use as input to Figure 9.

Table V. Attenuation Integral for μh of 10

Case	p	q	$\mu t = 2$ $\times 10^3$	$\mu t = 4$ $\times 10^4$	$\mu t = 6$ $\times 10^5$	$\mu t = 8$ $\times 10^6$	$\mu t = 10$ $\times 10^7$	$\mu t = 14$ $\times 10^9$	$\mu t = 18$ $\times 10^{11}$	$\mu t = 25$ $\times 10^{14}$
I	0	0	48.809	37.677	35.851	37.452	41.281	55.656	80.361	53.489
II	0	1/2	31.339	28.778	29.567	32.253	36.546	50.444	74.040	49.997
III	0	3/4	25.046	24.091	25.532	28.470	32.791	-	-	-
IV	0	1	20.699	20.459	22.140	25.089	29.270	42.123	63.607	44.376
V	0	2	12.158	12.374	13.861	16.200	19.415	29.199	45.647	33.343
VI	0	3	8.843	8.845	9.935	11.697	14.137	-	-	-
VII	0	4	7.201	6.990	7.778	9.136	11.051	16.984	27.126	20.492
VIII	0	5	6.267	5.893	6.464	7.540	9.089	13.943	22.292	16.908
IX	1/8	1/8	43.130	35.683	34.670	36.567	40.523	54.429	78.623	52.242
X	1/4	1/4	34.453	31.386	31.784	34.268	38.486	52.486	76.451	51.208
XI	1/4	1/2	27.184	26.544	27.975	30.934	35.345	-	-	-
XII	1/4	3/4	21.930	22.329	24.225	27.355	31.754	-	-	-
XIII	1/2	1/2	21.841	22.675	24.771	28.033	32.547	46.298	69.175	47.566
XIV	1/2	3/4	17.819	19.214	21.558	24.878	29.317	-	-	-
XV	1	1	10.379	12.142	14.468	17.486	21.374	32.778	51.599	37.713
XVI	1	2	6.185	7.525	9.266	11.517	14.423	-	-	-
XVII	1	3	4.329	5.334	6.643	8.344	10.551	-	-	-
XVIII	2	2	3.739	4.730	6.016	7.685	9.855	16.354	27.411	21.788
XIX	2	3	2.627	3.367	4.333	5.594	7.243	-	-	-
XX	3	3	1.846	2.398	3.122	4.075	5.327	-	-	-

Table VI. Attenuation Integral for μh of 15

Case	p	q	$\mu t = 2$ $\times 10^3$	$\mu t = 4$ $\times 10^4$	$\mu t = 6$ $\times 10^5$	$\mu t = 8$ $\times 10^6$	$\mu t = 10$ $\times 10^7$
I	0	0	48.809	37.677	35.851	37.452	41.281
II	0	1/2	27.924	26.355	27.556	30.420	34.767
III	0	3/4	21.589	21.263	22.938	25.923	30.172
IV	0	1	17.473	17.589	19.339	22.202	26.180
V	0	2	10.009	10.137	11.415	13.435	16.214
VI	0	3	7.373	7.203	8.042	9.468	11.468
VII	0	4	-	-	-	-	-
VIII	0	5	-	-	-	-	-
IX	1/8	1/8	-	-	-	-	-
X	1/4	1/4	30.765	29.181	30.167	32.917	37.255
XI	1/4	1/2	23.097	23.543	25.461	28.636	33.112
XII	1/4	3/4	18.027	19.103	21.269	24.460	28.785
XIII	1/2	1/2	17.674	19.218	21.652	25.039	29.538
XIV	1/2	3/4	13.941	15.713	18.188	21.478	25.760
XV	1	1	7.453	9.062	11.130	13.785	17.195
XVI	1	2	4.205	5.278	6.666	8.464	10.794
XVII	1	3	2.872	13.637	4.631	5.926	7.613
XVIII	2	2	2.380	3.087	4.011	5.222	6.810
XIX	2	3	1.619	2.119	2.778	3.647	4.792
XX	3	3	1.093	1.445	1.912	2.530	3.352

Table VII. Geometry Shielding Factor for μh of 10

Case	$\mu t = 2$	$\mu t = 4$	$\mu t = 6$	$\mu t = 8$	$\mu t = 10$	$\mu t = 14$	$\mu t = 18$	$\mu t = 25$
I	1.0000	1.0000	1.0000	1.0000	1.0000	1.0000	1.0000	1.0000
II	0.6420	0.7638	0.8427	0.8612	0.8853	0.9064	0.9214	0.9347
III	0.5131	0.6394	0.7122	0.7602	0.7943	-	-	-
IV	0.4241	0.5430	0.6176	0.6699	0.7090	0.7568	0.7915	0.8296
V	0.2491	0.3284	0.3866	0.4326	0.4703	0.5246	0.5680	0.6233
VI	0.1812	0.2348	0.2771	0.3123	0.3425	-	-	-
VII	0.1475	0.1855	0.2169	0.2439	0.2677	0.3052	0.3376	0.3830
VIII	0.1284	0.1564	0.1803	0.2013	0.2202	0.2505	0.2774	0.3161
IX	0.8836	0.9471	0.9671	0.0763	0.9816	0.9780	0.9784	0.9767
X	0.7058	0.8330	0.8866	0.9150	0.9323	0.9431	0.9514	0.9573
XI	0.5569	0.7045	0.7803	0.8259	0.8562	-	-	-
XII	0.4493	0.5926	0.6756	0.7304	0.7692	-	-	-
XIII	0.4475	0.6018	0.6910	0.7485	0.7884	0.8319	0.8608	0.8892
XIV	0.3651	0.5100	0.6013	0.6642	0.7102	-	-	-
XV	0.2126	0.3223	0.4036	0.4669	0.5178	0.5890	0.6421	0.7050
XVI	0.1267	0.1997	0.2585	0.3075	0.3494	-	-	-
XVII	0.0887	0.1416	0.1853	0.2228	0.2556	-	-	-
XVIII	0.0766	0.1255	0.1678	0.2052	0.2387	0.2938	0.3411	0.4073
XIX	0.0538	0.0894	0.1209	0.1494	0.1754	-	-	-
XX	0.0378	0.0636	0.0871	0.1088	0.1291	-	-	-

Table VIII. Geometry Shielding Factor for μh of 15

Case	$\mu t = 2$	$\mu t = 4$	$\mu t = 6$	$\mu t = 8$	$\mu t = 10$
I	1.0000	1.0000	1.0000	1.0000	1.0000
II	0.5721	0.6995	0.7686	0.8122	0.8422
III	0.4423	0.5644	0.6398	0.6931	0.7309
IV	0.3580	0.4668	0.5394	0.5928	0.6342
V	0.2051	0.2691	0.3184	0.3587	0.3928
VI	0.1510	0.1912	0.2243	0.2528	0.2778
VII	-	-	-	-	-
VIII	-	-	-	-	-
IX	-	-	-	-	-
X	0.6303	0.7745	0.8414	0.8790	0.9025
XI	0.4732	0.6249	0.7102	0.7646	0.8021
XII	0.3693	0.5070	0.5932	0.6531	0.6973
XIII	0.3621	0.5101	0.6039	0.6686	0.7155
XIV	0.2856	0.4170	0.5073	0.5734	0.6240
XV	0.1527	0.2405	0.3104	0.3681	0.4165
XVI	0.0861	0.1401	0.1859	0.2260	0.2615
XVII	0.0588	0.0965	0.1292	0.1582	0.1844
XVIII	0.0488	0.0819	0.1119	0.1394	0.1650
XIX	0.0332	0.0563	0.0775	0.0974	0.1161
XX	0.0224	0.0384	0.0533	0.0676	0.0812

Table IX. Geometry Factor for Silo Case

μr_o	μh	μt	GF	GF'
10	15	2	0.4404	0.4184
		4	0.6421	0.6184
		6	0.7675	0.7466
		10	0.9002	0.8877
		14	0.9566	0.9500
		18	0.9809	0.9777
10	25	2	0.1945	0.1904
		4	0.3157	0.3100
		6	0.4167	0.4101
		10	0.5748	0.5676
		14	0.6893	0.6827
		18	0.7727	0.7670
10	35	2	0.1047	0.1043
		4	0.1763	0.1757
		6	0.2410	0.2402
		10	0.3544	0.3535
		14	0.4505	0.4495
		18	0.5322	0.5311
10	50	2	0.0532	0.0532
		4	0.0914	0.0914
		6	0.1273	0.1273
		10	0.1943	0.1943
		14	0.2560	0.2560
		18	0.3128	0.3128

Table IX. (Continued)
(page 2 of 5 pages)

μr_o	μh	μt	GF	GF'
10	75	2	0.0246	0.0246
		4	0.0426	0.0426
		6	0.0600	0.0600
		10	0.0936	0.0936
		14	0.1258	0.1258
		18	0.1568	0.1568
10	100	2	0.0137	0.0137
		4	0.0239	0.0239
		6	0.0339	0.0339
		10	0.0531	0.0531
		14	0.0720	0.0720
		18	0.0904	0.0904
15	15	2	0.6837	0.6677
		4	0.8692	0.8586
		6	0.9448	0.9390
		10	0.9898	0.9885
		14	0.9981	0.9979
		18	0.9992	0.9991
14	25	2	0.3704	0.3636
		4	0.5569	0.5489
		6	0.6859	0.6783
		10	0.8409	0.8354
		14	0.9190	0.9156
		18	0.9586	0.9567
15	35	2	0.2263	0.2250
		4	0.3473	0.3454
		6	0.4549	0.4528
		10	0.6185	0.6163
		14	0.7325	0.7306
		18	0.8123	0.8107

Table IX. (Continued)
(page 3 of 5 pages)

μr_o	μh	μt	GF	GF'
15	50	2	0.1141	0.1141
		4	0.1915	0.1915
		6	0.2609	0.2608
		10	0.3812	0.3811
		14	0.4815	0.4814
		18	0.5656	0.5653
15	75	2	0.0532	0.0532
		4	0.0914	0.0914
		6	0.1273	0.1273
		10	0.1943	0.1943
		14	0.2559	0.2559
		18	0.3128	0.3128
15	100	2	0.0305	0.0305
		4	0.0528	0.0528
		6	0.0741	0.0741
		10	0.1165	0.1165
		14	0.1540	0.1540
		18	0.1912	0.1912
20	15	2	0.8320	0.8247
		4	0.9582	0.9555
		6	0.9893	0.9885
		10	0.9993	0.9992
		14	0.9999	0.9999
		18	0.9999	0.9999
20	25	2	0.5367	0.5300
		4	0.7427	0.7367
		6	0.8555	0.8511
		10	0.9538	0.9519
		14	0.9851	0.9844
		18	0.9952	0.9949

Table IX. (Continued)
(page 4 of 5 pages)

μr_o	μh	μt	GF	GF'
20	35	2	0.3407	0.3385
		4	0.5196	0.5170
		6	0.6493	0.6467
		10	0.8097	0.8077
		14	0.8968	0.8955
		18	0.9439	0.9431
20	50	2	0.1906	0.1904
		4	0.3102	0.3100
		6	0.4104	0.4101
		10	0.5680	0.5676
		14	0.6830	0.6827
		18	0.7672	0.7670
20	75	2	0.0920	0.0920
		4	0.1556	0.1556
		6	0.2137	0.2137
		10	0.3173	0.3173
		14	0.4069	0.4069
		18	0.4846	0.4846
20	100	2	0.0532	0.0532
		4	0.0914	0.0914
		6	0.1273	0.1273
		10	0.1943	0.1943
		14	0.2559	0.2559
		18	0.3128	0.3128
25	15	2	0.9137	0.9113
		4	0.9876	0.9872
		6	0.9982	0.9981
		10	0.9999	0.9999
		14	0.9999	0.9999
		18	0.9999	0.9999

Table IX. (Continued)
(page 5 of 5 pages)

μr_o	μh	μt	GF	GF'
25	25	2	0.6723	0.6677
		4	0.8632	0.8586
		6	0.9406	0.9390
		10	0.9889	0.9885
		14	0.9979	0.9979
		18	0.9996	0.9996
25	35	2	0.4628	0.4605
		4	0.6667	0.6643
		6	0.7911	0.7891
		10	0.9172	0.9162
		14	0.9670	0.9666
		18	0.9868	0.9866
25	50	2	0.2759	0.2756
		4	0.4332	0.4328
		6	0.5543	0.5538
		10	0.7232	0.7228
		14	0.8278	0.8275
		18	0.8927	0.8925
25	75	2	0.1383	0.1383
		4	0.2298	0.2298
		6	0.3102	0.3102
		10	0.4452	0.4452
		14	0.5358	0.5358
		18	0.6408	0.6408
25	100	2	0.0814	0.0814
		4	0.1383	0.1383
		6	0.2000	0.2000
		10	0.2932	0.2932
		14	0.3753	0.3753
		18	0.4419	0.4419

Appendix B

EXAMPLES OF COMPUTED GEOMETRY FACTORS FOR VARIOUS SHELTERS

1. Horizontal Cylinder

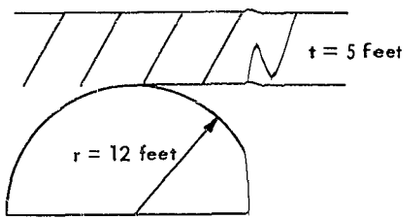

$$p = \frac{h}{c} = \frac{r}{r} = 1$$

$$F = \frac{p^2}{2} = \frac{1}{2}$$

$$\frac{t}{t + Fh} = \frac{5}{5 + \frac{1}{2}(12)} = 0.455$$

2. Sphere

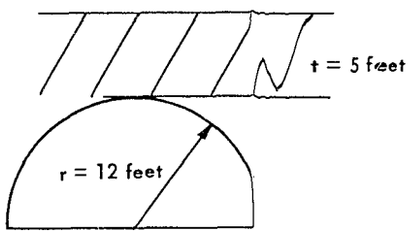

$$p = \frac{h}{c} = 1$$

$$q = \frac{h}{b} = 1$$

From Figure 7, F = 1

$$\frac{t}{t + Fh} = \frac{5}{5 + 12} = 0.294$$

Thus, from Figure 6, GF = 0.348

3. Ellipsoid

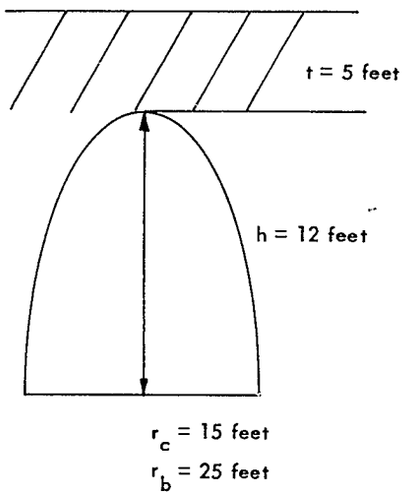

$$p = \frac{h}{c} = \frac{12}{15} = 0.8$$

$$q = \frac{h}{b} = \frac{12}{25} = 0.48$$

$$\frac{p^2 + q^2}{2} = \frac{0.64 + 0.23}{2} = 0.435$$

From Figure 7, F = 0.475

$$\frac{t}{t + Fh} = \frac{5}{5 + (0.475)\ 12} = 0.467$$

Thus, from Figure 6, GF = 0.51

4. Cattle Pass

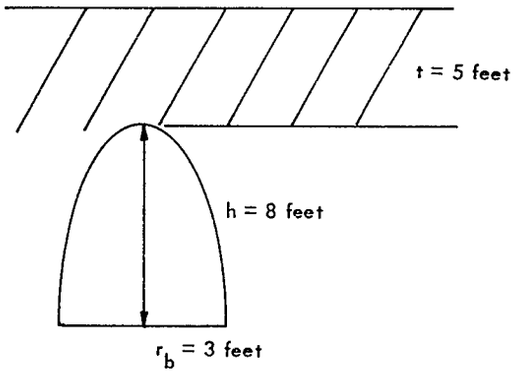

$$p = \frac{h}{c} = 0$$

$$q = \frac{h}{b} = \frac{8}{3} = 2.677$$

$$\frac{q^2}{2} = 3.56$$

From Figure 7, F = 3

$$\frac{t}{t + Fh} = \frac{5}{5 + 3(8)} = 0.172$$

From Figure 6, GF = 0.225

5. Silo

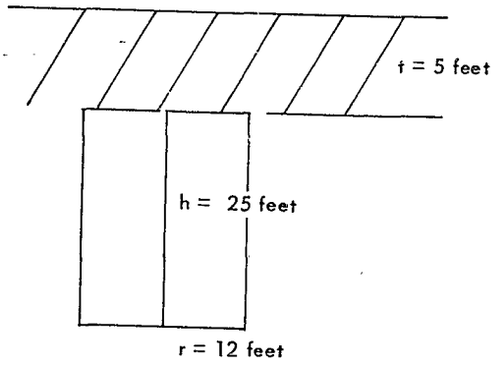

$$\frac{r_o}{h} = 0.48$$

A. Fallout: $E \cong 1.0$ Mev

Soil: $\rho = 1.7$ gm/cc

From Table II: $\mu_i = 3.00\ ft^{-1}$
$\mu_i t = 3\ (5) = 15$

From Figure 9, $GF = 0.825$

B. Initial Radiation: $E \cong 6.0$ Mev

Soil: $\rho = 1.7$ gm/cc

From Table II: $\mu_i = 1.27\ ft^{-1}$
$\mu_i t = 1.27\ (5) = 6.35$

From Figure 9, $GF = 0.565$

DISTRIBUTION LIST

No. of Copies	SNDL Code	
10		Chief, Bureau of Yards and Docks
		BuDocks Standard Distribution
1	23A	Naval Forces Commanders (Taiwan Only)
2	39B	Construction Battalions
9	39D	Mobile Construction Battalions
3	39E	Amphibious Construction Battalions
2	39F	Construction Battalion Base Units
1	A2A	Chief of Naval Research - Only
2	A3	Chief of Naval Operations (Op-07, Op-04)
5	A5	Bureaus
3	B3	Colleges
2	F4	Laboratory ONR (Washington, D. C. Only)
1	E16	Training Device Center
8	F9	Station - CNO (Boston; Key West; New Orleans; San Juan; Long Beach; San Diego; Treasure Island; and Rodman, C. Z. Only)
5	F17	Communication Station (San Juan; San Francisco; Pearl Harbor; Adak, Alaska; and Guam only)
1	F21	Administration Command and Unit CNO (Saipan only)
2	F40	Communication Facility (Pt Lyautey and Japan only)
1	F41	Security Station
2	F42	Radio Station (Oso and Cheltenham only)
1	F48	Security Group Activities (Winter Harbor only)
8	H3	Hospital (Chelsea; St. Albans; Portsmouth, Va; Beaufort; Great Lakes; San Diego; Oakland; and Camp Pendleton only)
1	H6	Medical Center
2	J1	Administration Command and Unit-BuPers (Great Lakes and San Diego only)
1	J3	U. S. Fleet Anti-Air Warfare Training Center (Virginia Beach only)
2	J4	Amphibious Bases
1	J19	Receiving Station (Brooklyn only)
1	J34	Station - BuPers (Washington, D. C. only)
1	J37	Training Center (Bainbridge only)
1	J46	Personnel Center
1	J48	Construction Training Unit
1	J60	School Academy

Distribution List (Cont'd)

No. of copies	SNDL Code	
1	J65	School CEC Officers
1	J84	School Postgraduate
1	J90	School Supply Corps
1	J95	School War College
1	J99	Communication Training Center
11	L1	Shipyards
4	L7	Laboratory - BuShips (New London; Panama City; Carderock; and Annapolis only)
5	L26	Naval Facilities - BuShips (Antigua; Turks Island; Barbados; San Salvador; and Eleuthera only)
1	L30	Submarine Base (Groton, Conn. only)
2	L32	Naval Support Activities (London & Naples only)
2	L42	Fleet Activities - BuShips
4	M27	Supply Center
7	M28	Supply Depot (Except Guantanamo Bay; Subic Bay; and Yokosuka)
2	M61	Aviation Supply Office
3	N1	BuDocks Director, Overseas Division
42	N2	Public Works Offices
7	N5	Construction Battalion Center
5	N6	Construction Officer-in-Charge
1	N7	Construction Resident-Officer-in-Charge
12	N9	Public Works Center
1	N14	Housing Activity
2	R9	Recruit Depot
[illegible]	[illegible]	[illegible] Installations (Albany and Barstow only)
1	R20	Marine Corps Schools, Quantico
3	R64	Marine Corps Base
1	R66	Marine Corps Camp Detachment (Tengan only)
7	W1A1	Air Station
35	W1A2	Air Station
9	W1B	Air Station Auxiliary
5	W1C	Air Facility (Phoenix; Monterey; Oppama; Naha; and Naples only)
3	W1E	Marine Corps Air Station (Except Quantico)
1	W1F	Marine Corps Auxiliary Air Station
8	W1H	Station - BuWeps (Except Rota)

No. of copies	
1	Chief of Staff, U. S. Army, Chief of Research and Development, Department of the Army, Washington 25, D. C.
1	Office of the Chief of Engineers, Asst. Chief of Engineering for Civil Works, Department of the Army, Washington 25, D. C.
1	Chief of Engineers, Department of the Army, Attn: Engineering R & D Division, Washington 25, D. C.
1	Commanding Officer, Engineering R & D Laboratories, Attn: Technical Intelligence Branch, Fort Belvoir, Virginia
1	Commanding General, Wright Air Development Center, Air Research and Development Command, Wright-Patterson Air Force Base, Ohio
1	Deputy Chief of Staff, Development, Director of Research and Development, Department of the Air Force, Washington
1	President, Marine Corps Equipment Board, Marine Corps Schools, Quantico, Virginia
1	Director, National Bureau of Standards, Department of Commerce, Connecticut Avenue, Washington, D. C.
10	Armed Services Technical Information Agency, Arlington Hall Station, Arlington 12, Virginia
1	Deputy Chief of Staff, Research and Development Headquarters, U. S Marine Corps
3	Headquarters, USAF, Directorate of Civil Engineering, Attn: AFOCE ! S, Washington 25, D. C.
2	Commander, Headquarters, Air Research and Development Command, Andrews Air Force Base, Washington 25, D. C.
2	Office of the Director, U. S. Coast and Geodetic Survey, Washington 25, D. C.
2	Library of Congress, Washington 25, D. C.
10	Director, Office of Technical Services, Department of Commerce, Washington 25, D. C.
	NCEL Standard Distribution
2	Director of Defense Research and Engineering, Department of Defense, Washington 25, D. C.
2	Director, Division of Plans and Policies, Headquarters, U. S. Marine Corps, Washington 25, D. C.
	[illegible], Bureau of Reclamation, Washington 25, D. C.
2	Commanding Officer, U. S. Naval Construction Battalion Center, Attn: Technical Division, Code 141, Port Hueneme, California
2	Commanding Officer, U. S. Naval Construction Battalion Center, Attn: Materiel Department, Code 142, Port Hueneme, California
1	Commanding Officer (Patent Dept.), Office of Naval Research Branch Office, 1030 E. Green Street, Pasadena, California

Distribution List (Cont'd)

No. of copies	
	NCEL Supplemental Distribution
1	Commandant, Industrial College of the Armed Forces, Washington, D. C.
1	Commandant, U. S. Armed Forces Staff College, U. S. Naval Base, Norfolk, Va.
1	Chief, Bureau of Ships, Attn: Chief of Research and Development Division, Navy Department, Washington, D. C.
1	Officer in Charge, U. S. Navy Unit, Rensselaer Polytechnic Institute, Troy, N. Y.
1	Chief Bureau of Naval Weapons, Attn: Research Division, Navy Department, Washington, D. C.
1	Commander, Pacific Missile Range, Attn: Technical Director, Point Mugu, Calif.
1	Commanding Officer, U. S Naval Unit, U. S. Army Chemical Corps School, Fort McClellan, Ala.
1	Deputy Chief of Staff, Research & Development Headquarters, U. S. Marine Corps, Washington D. C.
1	Deputy CCMLO for Scientific Activities, Washington, D .C.
1	Chief of Ordnance, U. S. Army, Attn: Research & Development Laboratory, Washington, D. C.
1	U. S. Army, Attn: Director of Research and Development Group, Washington, D. C.
1	Directorate of Medical Research, Chemical Warfare Board, Army Chemical Center, Md.
1	U. S. Army Corps of Engineers, Office of the District Engineer, St. Paul District, 1217 U. S. P. O. and Customs House, St. Paul, Minn.
1	Snow, Ice, and Permafrost Research Establishment, Corps of Engineers, U. S. Army, 1215 Washington Avenue, Willmette, Ill.
1	Taft Sanitary Engineering Center USPHS, 4676 Columbia Parkway, Cincinnati, Ohio
1	Commander, Air Research & Development Command, Attn: Library, Andrews Air Force Base, Washington, D. C.
1	Directorate of Research, Air Force Special Weapons Center, Kirtland Air Force Base, N. M.
1	Commanding Officer, Biological Warfare Laboratories, Fort Detrick, Frederick, Md.
1	Sandia Corporation, Attn: Classified Document Division, Box 5800, Albuquerque, N. M.
1	Operation Crust, University of California, Richmond Field Station, Berkeley, Calif.
1	Library, Engineering Department, Stanford University, Stanford, Calif.
1	Library, Harvard University, Graduate School of Engineering, Cambridge, Mass.
1	Director, Engineering Research Institute, University of Michigan, Ann Arbor, Mich.
1	Library, Engineering Department, University of California, 405 Hilgard Avenue, Los Angeles
1	Library, University of Southern California, University Park Los Angeles
1	Director, Marine Laboratory, University of Miami, Coral Gables, Fla.
1	Director, Soil Physics Laboratory, Department of Engineering, Attn: Library, Princeton University, Princeton, N. J.
1	Chief, Bureau of Yards and Docks, Code D-230, Washington, D. C.
1	Mr. W. R. Perret, 5112, Sandia Corporation, Sandia Base, Albuquerque, N. M.
1	Dr. N. M. Newmark, Civil Engineering Hall, University of Illinois, Urbana, Ill.
1	Mr. Fred Sauer, Physics Department, Stanford Research Institute, Menlo Park, Calif.
1	Dr. Harold Brode, RAND Corporation, 1700 Main Street, Santa Monica, Calif.

Distribution List (Cont'd)

No. of copies	
1	Mr. Kenneth Kaplan, Broadview Research Corporation, 1811 Trousdale Drive, Burlingame, Calif.
1	Prof. J. Neils Thompson, Civil Engineering Department, University of Texas, Austin, Tex.
1	Mr. G. L. Arbuthnot, Waterways Experiment Station, Post Office Box 631, Vicksburg, Miss.
1	Mr. William J. Taylor, Terminal Ballistics Laboratory, Aberdeen Proving Ground, Aberdeen Proving Ground, Md.
1	Dr. T. H. Schiffman, Armour Research Foundation of Illinois Institute of Technology, Technology Center, Chicago, Ill.
1	Chiefof Engineers, Department of the Army, Washington, D. C.
1	Mr. Eric Wang, Air Force Special Weapons Center, Kirtland AFB, Albuquerque, N. M.
1	Commander, Air Force Ballistic Missile Division, Air Research and Development Command, Attn: Dr. George Young, Post Office Box 262, Inglewood, Calif.
1	Dr. James O. Buchanan, Office of Civil and Defense Mobilization, Battle Creek, Mich.
1	Mr. L. Neal FitzSimons, Office of Civil and Defense Mobilization, Winder Building, Washington, D. C.
1	Mr. E. E. Shalowitz, Protective Construction, GSA Building, 19th and F Street, N. W., Washington, D. C.
1	Lt. Col. Russell J. Hutchinson, 052921, Office of Area Engineer, Saudi Arabia, U. S. A. Engineer District, Trans-East, APO 616, New York
1	Capt. A. B. Chilton, CEC, USN, U. S. Naval Civil Engineering Laboratory, Port Hueneme, Calif.
1	Cdr. C. A. Grubb, CEC, USN, Public Works Center, Navy No. 128, FPO, San Francisco
1	Capt. W. M. McLellone, CEC, USN, Public Works Office, U. S. Naval Base, Charleston, S. C.
1	Capt L. N. Saunders, Jr., CEC, USN, Bureau of Yards and Docks, Code D-400, Washington, D. C.
1	Cdr. J. F. Clarke, CEC, USN, Area Public Works Office, Chesapeake, U. S. Naval Weapons Plant [illegible] D. C.
1	Ldcr. [illegible] [illegible] Naval District, Navy No. 128, FPO San Francisco
1	Mr. G. H. Albright, The Pennsylvania State University, College of Engineering and Architecture, University Park, Penn.
1	Capt. J. H. Barker, Jr., CEC, USN, U. S. Naval Missile Center, Point Mugu, Calif.
1	Cdr. W. J. Christenson CEC, USN, Bureau of Yards and Docks, Code D-440, Washington, D. C.
1	Capt. J. H. Lofland, Jr., CEC, USN, Pearl Harbor Naval Shipyard, Navy No. 128, FPO, San Francisco
1	Capt. W. A. McManus, CEC, USN, U. S. Naval Air Station, Norfolk, Va.
1	Ldcr. J. D. Andrews, CEC, USN, Defense Atomic Support Agency, Washington, D. C.
1	Cdr. D. P. Cunning, CEC, USN, District Public Works Office, 4th Naval District, Naval Base, Philadelphia, Penn.
1	Ldcr. W. J. Francy, CEC, USN, Bureau of Yards and Docks, Code D-500, Washington, D. C.
1	Ldcr. F. W. Galbraith, CEC, USN, U. S. Naval Air Station, North Island, San Diego